

# Phase Shift Keying on the Hypersphere: Power-Efficient MIMO Communications

Christoph Rachinger, Ralf R. Müller and Johannes B. Huber  
Friedrich-Alexander-University Erlangen-Nürnberg, Germany  
Email: {christoph.rachinger, ralf.r.mueller, johannes.huber}@fau.de

**Abstract**—The modulation scheme Phase Shift Keying on the Hypersphere (PSKH), a generalization of conventional Phase Shift Keying (PSK) for Multiple-Input Multiple-Output (MIMO) systems, is introduced. In PSKH, constellation points are distributed over a multidimensional hypersphere. The use of such constellations with Peak-To-Average-Sum-Power-Ratio (PASPR) of 1 allows to use load-modulated transmitters which require much smaller backoff, which in turn results in a higher power efficiency. In this paper we discuss several methods how to generate PSKH constellations and compare their performance. After applying conventional Pulse-Amplitude Modulation (PAM), the PASPR of the continuous time PSKH signal depends on the choice of the pulse shaping method. This choice also influences bandwidth and power efficiency of a PSKH system. In order to reduce the PASPR of the continuous transmission signal, we use spherical interpolation to generate a smooth signal over the hypersphere and present the corresponding receiver. Additionally, complexity reduction techniques are proposed and compared. Finally, we discuss the methods presented in this paper regarding their trade-offs with respect to PASPR, bandwidth, power efficiency and receiver complexity.

**Index Terms**—Multiple-input multiple-output systems, wireless communications, peak-to-average-power, load-modulation.

## I. INTRODUCTION

POWER efficiency has been one of the driving forces behind the development of current communication technologies. Unfortunately, one of the main sources of power consumption are amplifiers operating at low power efficiency. This holds even for state-of-the-art amplifiers, which cannot be operated at their optimal power level, because signals with suboptimal Peak-To-Average-Power-Ratio (PAPR), i.e. a  $\text{PAPR} > 1$ , require a certain backoff of the amplifier to avoid serious clipping. Constant envelope modulation schemes such as continuous phase modulation (CPM) provide an optimal PAPR and reduce the backoff compared to other modulation schemes, such as the widely used QAM [1]. While this improves the power efficiency of a transmission system, the bandwidth efficiency suffers: Since the radius in the complex plane is fixed for constant envelope transmission, phase remains the only degree of freedom to represent information. This results in a rate loss compared to QAM, which is why constant envelope modulation did not receive much attention since the development of GSM-Mobile Communication, a system employing GMSK, a variant of CPM.

The use of MIMO systems allows for another method to increase power efficiency: Not the PAPR, but the Peak-to-Average-Sum-Power-Ratio (PASPR) of a vector-valued signal

can determine the required amplifier backoff. For an arbitrary vector-valued function  $\mathbf{x}(t) \in \mathbb{C}^n$ , this quantity is defined as

$$\text{PASPR}(\mathbf{x}(t)) = \frac{\max_t \|\mathbf{x}(t)\|^2}{\mathcal{E}\{\|\mathbf{x}(t)\|^2\}}. \quad (1)$$

The PASPR is a decisive factor when recently proposed load-modulated MIMO amplifiers are used [2], [3]. Since the degrees of freedom are reduced by only one for all antennas, the rate loss becomes smaller the more antennas are used [4]. For massive MIMO systems, the central limit theorem (CTL) guarantees that the PASPR of the continuous-time signal becomes optimal as long as the data points are distributed on a multidimensional hypersphere. We call these constellations *Phase Shift Keying on the Hypersphere* (PSKH), because it is a natural extension of ordinary PSK. In conventional MIMO with only a handful of antennas, large fluctuations of the continuous transmit signal are still possible and therefore the PASPR is far from being optimal. Thus some more adaptations are necessary in order to reduce the PASPR of the transmission signal.

The rest of this paper is organized as follows: In Sec. II we introduce our system model. Unlike in PSK, there are multiple ways to construct a constellation. Thus we discuss several algorithms to generate PSKH constellations and their advantages and disadvantages in Sec. III. Secs. IV and V presents two approaches to reduce the PASPR in detail. This includes receiver structures for the corresponding signals as well as numerical results for their performance. Sec. VI discusses how much the previously introduced approaches reduce the PASPR of the transmitter output signal and they affect the spectrum. Secs. VII compares the results from the previous sections from the perspective of bandwidth efficiency. The paper ends with a conclusion in Sec. VIII.

## II. SYSTEM MODEL

We define a PSKH constellations as a set of  $M = 2^{R_m}$  data points  $\mathcal{A} = \{\mathbf{a}_0, \dots, \mathbf{a}_{M-1} \mid \mathbf{a}_i \in \mathbb{C}^{n_T}, \|\mathbf{a}_i\| = \sqrt{E_s}\}$  where  $E_s$  is the energy per symbol,  $n_T$  is the number of transmit antennas and  $R_m$  the rate per modulation interval. Unless otherwise mentioned, these constellations are modulated using conventional PAM with a pulse shaping filter  $h(t)$  to generate the continuous-time transmitter output signal

$$\mathbf{s}(t) = \sum_{k=-\infty}^{\infty} \mathbf{x}[k]h(t - kT), \quad \mathbf{x}[k] \in \mathcal{A} \quad (2)$$

with the data sequence  $\langle \mathbf{x}[k] \rangle$ .

If  $h(t)$  is a  $\sqrt{N}$ yquist filter and the corresponding matched filter is applied at the receiver, the overall model is the well known discrete-time MIMO channel model

$$\mathbf{y}[k] = \mathbf{H}\mathbf{x}[k] + \mathbf{n}[k] \quad (3)$$

where  $\mathbf{x}[k] \in \mathbb{C}^{n_T}$ ,  $\mathbf{y}[k] \in \mathbb{C}^{n_R}$  are transmit and receive vector at time  $k$ , respectively,  $\mathbf{H} \in \mathbb{C}^{n_T \times n_R}$  is the channel matrix and  $\mathbf{n}[k] \in \mathbb{C}^{n_R}$  is complex i.i.d. additive white Gaussian noise with variance  $\sigma^2$  per complex component.  $n_R$  and  $n_T$  denote the number of transmit and receive antennas respectively, but for the remainder of this paper we assume that  $n = n_R = n_T$  and omit the time index  $k$  unless confusion is possible. If other pulse shaping filters than  $\sqrt{N}$ yquist are used, it will be discussed in detail.

For this work, both the continuous and discrete time models (eqs. (2) and (3)) are important, because the first one determines the PASPR and bandwidth of the signal whereas the latter can be used for the detection of the transmitted sequence in the receiver.

Because every point in a PSKH constellation has energy  $E_s$  and uses  $\sqrt{N}$ yquist-impulses, the equivalent energy per bit information is given as  $E_s/R_m$ . If the entries of  $\mathbf{H}$  are i.i.d complex Gaussian random variables with unit variance, each antenna receives a signal energy of  $E_s$  per symbol and hence the total received energy over  $n$  receive antennas is  $nE_s$ . Thus average received energy per bit information over the two-sided noise-spectral density is given as

$$\frac{E_b}{N_0} = \frac{nE_s}{R_m\sigma^2}. \quad (4)$$

### III. PSKH CONSTELLATIONS

#### A. Constellation Construction

As explained in Sec. II, a PSKH constellation is a set of  $M = 2^{R_m}$  points on the hypersphere with radius  $\sqrt{E_s}$  representing  $R_m$  bits. The vectors  $\mathbf{a}_i \in \mathcal{A} \subset \mathbb{C}^n$  are  $n$ -dimensional corresponding to  $n$  transmit antennas in a MIMO system. We note that our PSKH constellations are also known as *spherical codes* in literature, but to our knowledge they have never been used to improve power efficiency of communication systems by means of PASPR reduction. Without further restrictions than the radius, there are many possible ways to create constellations, which might differ quite vastly in terms of quality. A reasonable measure for quality, as in all PAM schemes, is the minimum distance between signal points. Optimal codes in this sense and their analytic description, however, are known only for some restricted constellation sizes and dimensions [5].<sup>1</sup> Because of this we compare four different algorithms to generate PSKH constellations:

- *Equal Area Partitioning Algorithm* (EQPA) from [7]: Generates a constellation with equally sized areas, which are usually not the Voronoi regions of a data point.
- *k-means Clustering* (kMC) using the spherical k-means algorithm [8]: Generates a large number of uniformly

<sup>1</sup>Some examples of such optimal packings can be found in [6].

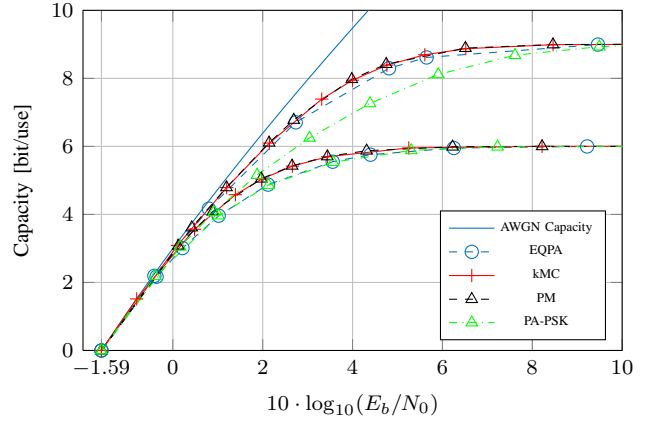


Fig. 1. Capacity of different constellations for a constellation size  $M = 64$  and  $M = 512$  points and  $n = 3$  antennas.

distributed points on the sphere, clusters them using the spherical k-means algorithm.

- *Potential Minimization* (PM): Generates particles on a sphere and minimizes the potential energy between particles. This can be done via a molecular dynamics simulation [9].
- *Per-Antenna PSK* (PA-PSK): Generates independent PSK constellations on each antenna, then scales them to fit the power constraint.

The algorithms can be distinguished in terms of construction complexity: EQPA and PA-PSK are analytic constructions, kMC and PM rely on numerical methods and are therefore more expensive to construct. Of course, such a construction needs to be done only once and can be computed offline. If construction is nonanalytic, it is further necessary to store the constellation in memory, which we think is reasonable to implement for  $R_m \lesssim 16$ . Additionally, it is possible to construct a constellation for only half the antennas and duplicate it, which results in a small degradation of quality.

In order to compare constellations with respect to their performance, we take a look at three different properties: Constellation-constrained capacities, minimum distance of the constellation (also known as *packing radius* in the context of spherical codes and packings) and error probabilities.

#### B. Capacity of PSKH

In [4], it was proven that the capacity of PSKH for unitary  $\mathbf{H}$  and continuous input is achieved for a uniform distribution on the hypersphere. In this section, we compare the capacities if the input is discrete and constrained to a certain size, but  $\mathbf{H}$  is still unitary. Fig. 1 shows the constellation constrained capacities for  $n = 3$  antennas and  $M = 64$  as well as  $M = 512$  points. As a baseline, we also plot the AWGN capacity  $C = 3 \log(1 + \text{SNR}_{\text{ch}})$  with  $\text{SNR}_{\text{ch}} = \frac{E_s}{n\sigma^2}$  being the SNR on each individual AWGN channel. The results are similar for different constellation and antenna array sizes, which is why we restrict ourselves to one exemplary case. The general result regarding capacities can be summarized as follows: PM and kMC have the best capacities with PM outperforming kMC by only approx. 0.01 dB. For a constellation size of 1 bit per

TABLE I  
AVERAGE AND TOTAL MINIMUM DISTANCE OF CONSTELLATIONS

	$d_{\min}$	$d_{\text{nb,avg}}$
EQPA, $M = 64$	0.6611	0.7282
kMC, $M = 64$	0.8674	0.9207
PM, $M = 64$	0.9139	0.9474
PA-PSK, $M = 64$	0.8165	0.8165
EQPA, $M = 512$	0.4654	0.5350
kMC, $M = 512$	0.5235	0.5767
PM, $M = 512$	0.5894	0.6217
PA-PSK, $M = 512$	0.4419	0.4419

real dimension, PA-PSK and EQPA lose up to 0.5 dB at a capacity of  $C = 5.5$  bit/use. If we increase the constellation size, PM and kMC still remain on top, EQPA reduces the loss to about 0.3 dB, whereas PA-PSK loses up to 2 dB compared to PM at  $C = 8.5$  bit/use. The reason for this big loss when increasing the constellation size is that PA-PSK is the only constellation where no form of global optimization, i.e., over all 6 dimensions, takes place. While a PSK constellation might be perfect on an individual antenna, increasing the total constellation size requires to use different constellations on each antenna. This can have devastating influence on the overall distance properties of the constellation. On the other hand, EQPA works in such a way that the distribution of points becomes more and more uniform as the constellation size increases. This algorithm profits from packing the hypersphere more dense.

Fig. 1 also shows that for coded transmission with a target rate well below  $R_m$ , the larger constellation can get very close to the AWGN capacity: Using  $M = 512$  points per constellation and assuming a code of rate  $R_c = \frac{1}{2}$ , i.e., a total rate of 4.5 bit, the gap to AWGN capacity is only approx. 0.1 dB. This fits nicely with a coded modulation rule of thumb stated in [10], [11] that 1 bit redundancy per real dimension for coding and shaping is sufficient to close most of the gap to capacity.

### C. Distance Properties

In order to compare the distance properties of the individual algorithms, Table I lists the *minimum distance* and *average neighbor distance* of a constellation defined as

$$d_{\min}(\mathcal{A}) = \min_{\substack{\mathbf{a}_i, \mathbf{a}_j \in \mathcal{A} \\ i \neq j}} \|\mathbf{a}_i - \mathbf{a}_j\| \quad (5)$$

and

$$d_{\text{nb,avg}}(\mathcal{A}) = \frac{1}{M} \sum_{i=0}^{M-1} \min_{\substack{\mathbf{a}_j \in \mathcal{A} \\ \mathbf{a}_i \neq \mathbf{a}_j}} \|\mathbf{a}_i - \mathbf{a}_j\|. \quad (6)$$

PSKH constellations, especially the ones which were generated numerically, often have asymmetric distance profiles: In conventional modulation schemes like PSK or QAM, every point has at least one neighbor which is the minimum distance apart. A lot of points (in PSK even all points) have the same distance profile to neighboring points. In PSKH, there may be only two neighboring points which are the minimum distance

apart, whereas all other points in the constellation only have neighbors which are further apart. This is the reason why we also include the average neighbor distance  $d_{\text{nb,avg}}$ . The conclusions that can be drawn from the two values given in Table I support the results gained from the constrained capacity analysis from the last subsection qualitatively, but it is not possible to estimate capacities from these values alone. The reason is that even for equal minimum distances, various constellations might have a significantly different overall distance profile, resulting in varying performances.

### D. Power Efficiency

In order to elaborate how the distance profile effects the power efficiency of PSKH constellations, Fig. 2 shows the symbol error rate (SER) for constellations when 3 antennas are used with constellation sizes  $M = 64$  and  $M = 512$ . Fig. 2a shows transmission over a vector AWGN channel, i.e.,  $\mathbf{H} = \mathbf{I}$ . For Fig. 2b, every element of  $\mathbf{H}$  is a complex i.i.d. Gaussian random variable with unit variance and we average over several thousand realizations. In both cases, one can observe that the error performance of the constellation is ordered according to the minimum distance of the constellation (like the capacity), but due to the size of a constellation and asymmetry of the distance profiles (see last section), a quantitative estimation is not developed yet.

*Remark:* We note that PA-PSK with  $M = 64$  for 3 antennas is regular 4-PSK on each antenna. Without further modification, an optimized constellation such as PM can give a substantial gain compared to 4-PSK/antenna of almost 1.5 dB on the vector AWGN channel. Such a channel is equivalent to subsequent transmissions over a regular AWGN channel. Constellations which achieve a coding gain by being spread over subsequent transmissions on a Single-Input Single-Output (SISO) channel are also known as *multidimensional constellations* [12]. Multidimensional constellations can be used to combat fading [13], [14], to exploit four available dimensions in optical communications [15], [16] and to introduce a more flexible trade-off between bandwidth the power efficiency of trellis-coded signals [17]. Such constellations are usually based on conventional 2-D modulation schemes or on some lattices, which generally does not result in fixed radius constellations. To our knowledge, no work has dealt with multidimensional constellations with fixed radius in MIMO systems to exploit load-modulation transmitter.

## IV. SINC<sup>2</sup> PULSE SHAPING

The simplest method to reduce the PASPR is to use pulse shaping filters which show better PASPR properties. PAM employing a sinc<sup>2</sup>( $t$ )-function<sup>2</sup> for pulse shaping shows very good properties even for very few antennas (see Sec. VI). This means that the continuous transmission signal is

$$\mathbf{s}(t) = \sum_{k=-\infty}^{\infty} \mathbf{x}[k] \text{sinc}^2\left(\frac{t - kT}{T}\right). \quad (7)$$

<sup>2</sup>We define  $\text{sinc}(x) = \sin(\pi x)/(\pi x)$  for  $x \neq 0$  and 1 otherwise.

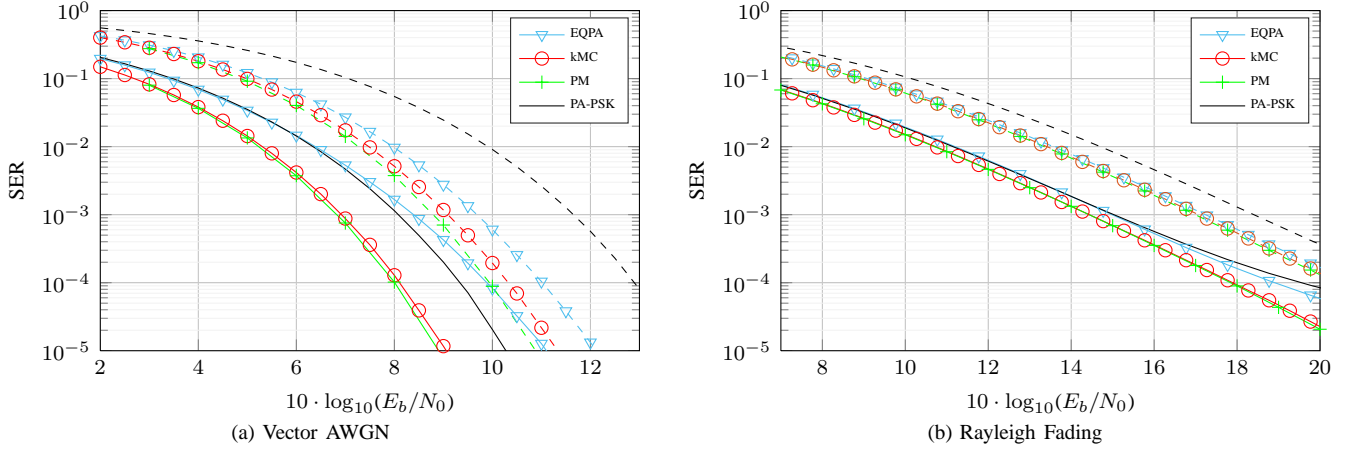


Fig. 2. Symbol error rate (SER) for transmission of  $R_m = 6$  (solid) or  $R_m = 9$  (dashed) bits per constellation point over a vector AWGN channel (a), and a Rayleigh fading channel (b). The system has  $n = 3$  antennas.

Since  $\text{sinc}^2$  is not a  $\sqrt{\text{Nyquist}}$ -function, some ISI has to be equalized at the receiver. This ISI is not generated by the channel, but only by the pulse shaping filter and its corresponding matched filter, i.e., there is no ISI between different receive antennas. Thus there is no need to make use of equalization techniques developed for MIMO ISI channels. Instead, we filter the received signal of each antenna using Forney's *Whitened Matched Filter* (WMF) [18]. ISI can then be expressed by a one-dimensional, causal minimum-phase filter  $h_W[i]$  and the resulting discrete time transmission model becomes

$$\mathbf{y}[k] = \mathbf{H} \sum_{i=0}^L h_W[i] \mathbf{x}[k-i] + \mathbf{n}[k] \quad (8)$$

with ISI-length  $L$ . ISI can be equalized with Maximum Likelihood Sequence Estimation (MLSE) using a vector-valued Viterbi Algorithm (VA) [19], Decision Feedback Equalization (DFE) or Delayed Decision Feedback Sequence Estimation (DDFSE) [20], which allows a performance trade-off between DFE and MLSE. In this specific case, almost all energy of  $h_W$  is stored in the very first coefficient  $h_W[0]$ , such that there is virtually no loss in terms of error probability when using DFE. Results of numerical simulations can be found in Fig. 3, there is virtually no loss between  $\text{sinc}^2$  pulse shaping with DFE (the worst equalization method in this scenario) and RRC pulse shaping (the best variant) in terms of power efficiency.

## V. SPHERICAL INTERPOLATION SIGNALING

Spherical Interpolation (SI) signaling tries to smoothen the transmission signal by forcing it onto the hypersphere also in between data samples. This is achieved by inserting interpolation points at a certain oversampling rate. The positive effect is a significantly reduced PASPR compared to conventional PAM because the signal becomes smoother and deviations from the hypersphere are reduced, especially zero-crossings. The disadvantages are ISI introduced by the interpolation points and thus an increased receiver complexity.

Before presenting our two approaches, we define spherical interpolation also known as SLERP (spherical

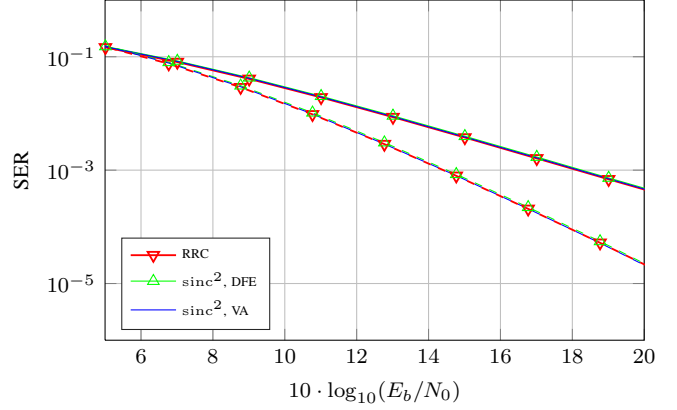


Fig. 3. Comparison of RRC and  $\text{sinc}^2$  pulse shaping. Transmission is over  $n = 2$  (solid) and  $n = 3$  (dashed) antennas with one bit per real dimension ( $M = 16$  and  $M = 64$ ).

interpolation) [21]: Given two points  $\mathbf{x}_1, \mathbf{x}_2 \in \mathbb{R}^N$  with  $\|\mathbf{x}_1\| = \|\mathbf{x}_2\| = 1$  and  $\cos(\theta) = \langle \mathbf{x}_1, \mathbf{x}_2 \rangle$ , for any  $0 \leq \tau \leq 1$ , the spherical interpolation of  $\mathbf{x}$  and  $\mathbf{y}$  is given as

$$\text{SI}(\mathbf{x}_1, \mathbf{x}_2, \tau) = \frac{\sin((1-\tau)\theta)}{\sin \theta} \mathbf{x}_1 + \frac{\sin(\tau\theta)}{\sin \theta} \mathbf{x}_2. \quad (9)$$

### A. $\frac{T}{2}$ -Pulse Shaping

As mentioned, introducing spherical interpolation samples introduces ISI. In order to simplify equalization, our first approach is to generate ISI by means of a  $\sqrt{\text{Nyquist}}$ -filter. This means we use a pulse shaping filter  $h(t)$  at twice the symbol rate. The resulting signal is

$$\begin{aligned} \mathbf{s}(t) = & \sum_{k=-\infty}^{\infty} \left( \mathbf{x}[k] h(2(t - kT)) \right. \\ & \left. + \text{SI} \left( \mathbf{x}[k], \mathbf{x}[k+1], \frac{1}{2} \right) h \left( 2 \left( t - \left( k + \frac{1}{2} \right) T \right) \right) \right) \end{aligned} \quad (10)$$

which is  $\sqrt{\text{Nyquist}}$  with respect to half the symbol rate. The corresponding matched filter is  $h^*(-2t)$ . Sampling with a rate

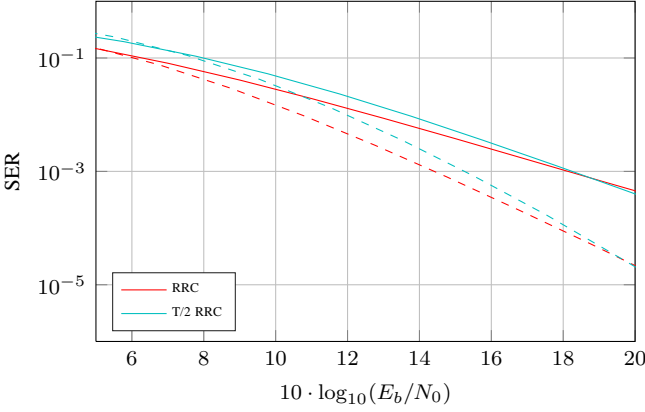


Fig. 4. Comparison of RRC and  $\frac{T}{2}$  pulse shaping. Transmission is over  $n = 2$  (solid) and  $n = 3$  (dashed) antennas with one bit per real dimension ( $M = 16$  and  $M = 64$ ).

of  $\frac{T}{2}$  gives a sequence of data points and interpolation values at the receiver.

To keep this system comparable with conventional PAM, both data and interpolation points contain only half the energy. Therefore it is necessary to use all points at the receiver to estimate the data sequence, otherwise half of the energy would be wasted. Data estimation for  $\frac{T}{2}$ -pulse shaping is done via the Viterbi algorithm.

It is obvious that this method has a huge disadvantage due to the much larger spectrum it occupies. The reason why we nevertheless include it in this comparison is that  $\frac{T}{2}$ -pulse shaping increases the slope of the error curve such that in the medium- to high-SNR regime it might still be a valid alternative given the largely reduced PASPR compared to conventional PAM. Results for this pulse shaping method are plotted in Fig. 4.

This increased slope can be explained by the linear transformation of the hypersphere induced by  $\mathbf{H}$ : At high SNRs, symbol errors will usually occur because the noise moves the data symbol into the decision region of a neighboring symbol. Symbol errors where the received symbol is in a decision region of a symbol from the opposite side of the hypersphere occur only rarely, because such points are farthest apart. If the receiver constellation  $\mathbf{H}\mathcal{A} = \{\mathbf{H}\mathbf{x} \mid \mathbf{x} \in \mathcal{A}\}$  is distorted enough, such errors may be much more likely because the distance between opposing points might be drastically reduced. In the case of  $\frac{T}{2}$ -pulse shaping, not only the distance between constellation points, but also the distance between interpolation points affects the performance of the system. For data points on opposing sides of the hypersphere,  $\frac{T}{2}$ -pulse shaping generates interpolation points which are usually far away from each other. This increases the total minimum distance and thus the performance of the transmission. The magnitude of this effect is dependent on  $\mathbf{H}$ . A good measure for this effect is the ratio  $\frac{\sigma_{\text{SVD},\text{max}}}{\sigma_{\text{SVD},\text{min}}}$  with  $\sigma_{\text{SVD},\text{max}}$  and  $\sigma_{\text{SVD},\text{min}}$  being the maximum and minimum singular values of the real representation of  $\mathbf{H}$ , respectively<sup>3</sup>. The two extreme cases would be  $\frac{\sigma_{\text{SVD},\text{max}}}{\sigma_{\text{SVD},\text{min}}} = 1$

<sup>3</sup>Every complex-valued model  $\mathbf{y} = \mathbf{H}\mathbf{x} + \mathbf{n}$  of dimension  $n$  can be transformed into an equivalent real-valued model of dimension  $2n$ , see e.g. [22].

in which  $\mathbf{H}\mathcal{A}$  would still be a hypersphere (possibly with a different radius) and  $\frac{\sigma_{\text{SVD},\text{max}}}{\sigma_{\text{SVD},\text{min}}} \rightarrow \infty$ . In the latter case, the  $n$ -dimensional hypersphere would be compressed down to fewer dimensions, effectively making opposing constellation points neighboring points.

### B. Spherical Interpolation

The main problem of  $\frac{T}{2}$ -pulse shaping is the large bandwidth due to the use of pulse shaping filters at higher frequency. In order to mitigate the problem, we combine SI with a conventional pulse shaping filter at its original frequency.

This method is characterized by the interpolation frequency  $f_{\text{IP}}$ : In each symbol interval, the original data point as well as  $f_{\text{IP}} - 1$  interpolation points are transmitted. The corresponding signal is

$$\mathbf{s}(t) = \sum_{k=-\infty}^{\infty} \left( \mathbf{x}[k] h(t - kT) + \sum_{l=1}^{f_{\text{IP}}-1} \mathbf{SI} \left( \mathbf{x}[k], \mathbf{x}[k+1], \frac{l}{f_{\text{IP}}} \right) h \left( t - \left( k + \frac{l}{f_{\text{IP}}} \right) T \right) \right). \quad (11)$$

At the receiver, we filter with the matched filter  $h^*(-t)$  followed by  $T$ -spaced sampling. Introducing the autocorrelation

$$\rho(\tau) = \int_{-\infty}^{\infty} h(t + \tau) h^*(t) dt, \quad (12)$$

the received discrete-time signal is

$$\mathbf{y}[k] = \mathbf{y}(kT) = \mathbf{H} \left( \sum_{\bar{k}=-\infty}^{\infty} \mathbf{x}[\bar{k}] \rho(kT - \bar{k}T) + \sum_{l=1}^{f_{\text{IP}}-1} \mathbf{SI} \left( \mathbf{x}[\bar{k}], \mathbf{x}[\bar{k}+1], \frac{l}{f_{\text{IP}}} \right) \cdot \rho \left( kT - \left( \bar{k} + \frac{l}{f_{\text{IP}}} \right) T \right) \right) + \mathbf{n}[k]. \quad (13)$$

By using a  $\sqrt{\text{Nyquist}}$ -pulse, the direct influence of adjacent data symbols may be suppressed and the resulting noise at the receiver is white, but the influence of the interpolation values inserted at a rate  $T_{\text{IP}} = T/f_{\text{IP}}$  remains. Thus ISI-equalization in form of MLSE via the VA has to be performed at the receiver. Fig. 5 shows the system model used at the receiver to estimate the data sequence. In order to do so, the VA has to be adapted in such a way that all  $f_{\text{IP}}$  vectors, which were transmitted during one symbol interval, are used to calculate the metric. Since  $T$ -spaced sampling is used, it is vital to use the contribution from the interpolation values, otherwise their energy would be wasted. As a result, the system would not be competitive.

The choice of  $f_{\text{IP}}$  provides a trade-off between receiver complexity and smoothness of the output signal (which in term improves PASPR and bandwidth, see Sec. VI). The results in Figs. 9 and 8 were generated using  $f_{\text{IP}} = 4$ . Increasing  $f_{\text{IP}}$  to 16 showed a 0.15 dB improvement in PASPR for a RRC with

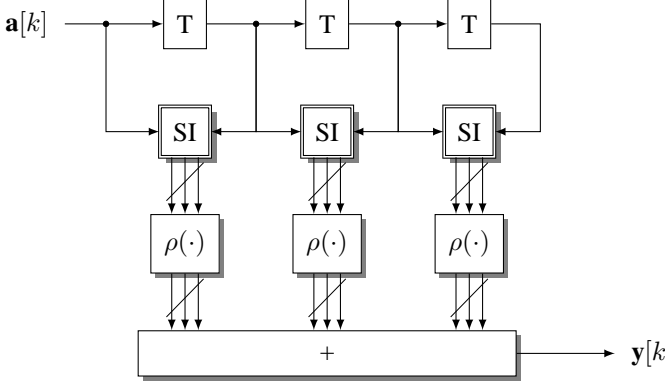


Fig. 5. System used to model the ISI produced by spherical interpolation transmission. An SI block calculates  $f_{IP}$  vectors and  $\rho(\cdot)$  weighs them with the autocorrelation of the pulse shaping filter. Thus each block processes all interpolation vectors within one symbol period. This model omits the channel matrix  $\mathbf{H}$  and noise  $\mathbf{n}$ .

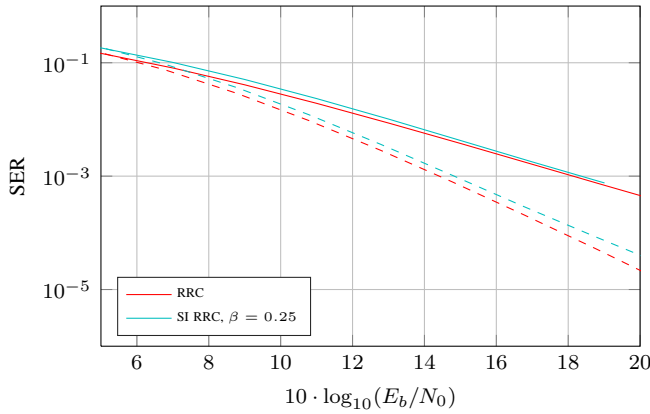


Fig. 6. Comparison of RRC and SI pulse shaping with  $f_{IP} = 4$ . Transmission is over  $n = 2$  (solid) and  $n = 3$  (dashed) antennas with one bit per real dimension ( $M = 16$  and  $M = 64$ ). The receiver used a Viterbi decoder with  $\nu = 2$  memory elements for  $n = 3$  antennas and  $\nu = 3$  memory elements for  $n = 2$  antennas.

$\beta = 0.25$ . The error probability is unaffected by increasing  $f_{IP}$ .

Fig. 6 shows numerical results for the spherical interpolation shaping using  $f_{IP} = 4$ . Detection was performed using the VA employing  $\nu = 3$  memory elements for the 16-ary constellation and  $\nu = 2$  memory elements for the 64-ary constellation (corresponding to 4096 states in both cases). Since such a huge number of states is in hard to implement in practice, we discuss some complexity reduction techniques and effects in the next section. Remaining pulse energy was equalized using DFE, which makes the overall scheme a Delayed Decision Feedback Sequence Estimation (DDFSE) [20]. For DDFSE, usually a prefilter is applied to make the overall impulse response minimum-phase, see e.g. [23]. In this case, the overall impulse response has a large linear phase portion. Additionally, most of its energy is concentrated around its center. After generating the minimum phase part of the overall impulse response it turned out that its energy spreads over a much wider interval than the original impulse response, which would require more memory elements in the VA to capture the same

amount of energy. This is computationally not feasible. It is thus advantageous to use the original filter instead of applying any prefilter to make the overall filter minimum phase and simply treat the influence of the first taps as noise.

SI pulse shaping shows excellent properties in terms of power efficiency. Depending on the pulse shape, the loss compared to a conventional PAM modulation employing a RRC filter is between 0 and 1 dB depending on the roll-off and the number of states: For a fixed number of states in the receiver, increasing the roll-off factor  $\beta$  for a RRC filter improves power efficiency, because more of the energy of  $\rho(t)$  is concentrated around the center. This is different from conventional PAM, where power efficiency is unaffected by the roll-off factor. In the next section we show how the gap between SI RRC and conventional RRC can be closed with reduced computational complexity.

### C. Complexity Reduction Techniques

As shown in Fig. 5, ISI needs to be equalized using the VA when spherical interpolation is used. It is usually sufficient to use only 2 or 3 delay elements to capture almost all energy of the pulse, the remaining energy at the end of the filter can be equalized by means of DDFSE. But since each delay element is  $M$ -ary, the number of states can become infeasible even for such a small number of elements. We thus compare system performance and complexity when using two different complexity reduction techniques: The well-known Reduced State Sequence Estimation (RSSE) [24] and an iterative application of the VA.

For RSSE, we use a Viterbi algorithm with  $\nu = 2$  memory elements and generate hypersymbols by using hypersymbols in the second delay element only. Combining different input symbols into a hypersymbol in the first element leads to large performance degradation due to two effects: Hypersymbols are calculated in advance based on the original constellation  $\mathcal{A}$ . We did this by numerically optimizing the minimum distance within each hyperstate. The effective constellation at the receiver, however, is  $\mathbf{H}\mathcal{A}$  which might have a drastically different distance profile than the constellation with originally optimal hypersymbols. The other negative impact is the fact that both the impulse response  $\rho(t)$  as well as its minimum-phase do not have monotonously decreasing values. The decision in the first delay element is thus based on only a small fraction of the total pulse energy.

Our second approach to reduce the complexity is to apply the Viterbi algorithm iteratively. This works well if the performance gap between the use of  $\nu$  and  $\nu+1$  memory elements is not too large. The idea behind it is that if each error pattern is a neighboring symbol of the correct signal point, it is sufficient to consider these neighboring symbols in future steps. This is a valid assumption if the SNR is sufficiently high. Our algorithm works as follows:

- 1) Initialize  $\nu = 1$ .
- 2) Run the Viterbi algorithm with one memory element.
- 3) For each estimate  $\hat{\mathbf{x}}[k]$ , find the  $n_{NB}$  nearest neighboring points.
- 4) Set  $\nu = \nu + 1$ .

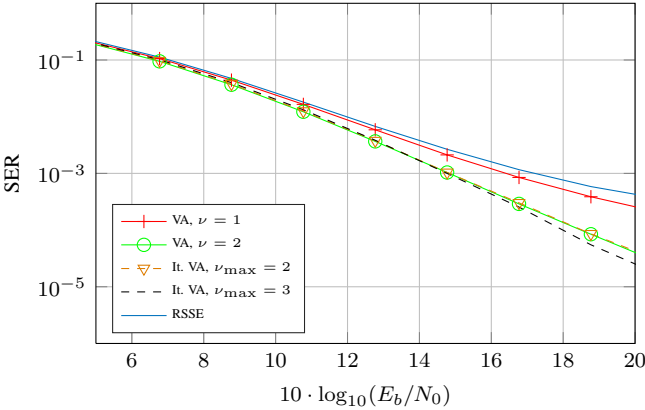


Fig. 7. Comparison of SI pulse shaping for  $n = 3$  antennas with a RRC pulse shape with  $\beta = 0.25$ . RSSE used a quaternary second delay element and  $n_{NB} = 4$  for all iterative variants.

- 5) Run the Viterbi algorithm with  $\nu$  memory elements, only allowing  $n_{NB} + 1$  points in each time step.
- 6) If  $\nu = \nu_{\max}$  finish, otherwise go back to 2.

The neighboring points can be calculated in advance and stored in a table. This works best if the neighboring points are taken from  $\mathbf{H}\mathcal{A}$ , but a reasonable performance can also be achieved if they are taken directly from  $\mathcal{A}$ , which reduces the overhead to recalculate them every time  $\mathbf{H}$  changes.

Fig. 7 shows the performance of a 64-ary alphabet transmitted via SI signaling with a RRC with  $\beta = 0.25$  employing  $n = 3$  antennas. The VA curve using two memory elements ( $\nu = 2$ ) is the same as in Fig. 6 and is our baseline. As a measure of complexity we count the number of branches in each time step

$$\Xi = \begin{cases} M^{\nu+1}, & \text{Standard VA} \\ M \cdot \prod_{i=1}^{\nu} M_i, & \text{VA, RSSE} \\ M^2 + \sum_{i=2}^{\nu_{\max}} (n_{NB,i} + 1)^{\nu_i+1}, & \text{Iterative VA.} \end{cases} \quad (14)$$

In this term,  $M_i$  is the number of possible values in the  $i$ -th delay element if RSSE is used (the number of hypersymbols) and  $\nu_i$  is the number of memory elements in the  $i$ -th iteration of the iterative VA. Table II shows the complexity for the algorithms used to create Fig. 7. The computational complexity for a VA with  $\nu = 2$  is already impractical. The iterative VA, however, provides the same performance as the VA with  $\nu = 2$  with only minor complexity increase compared to the VA with  $\nu = 1$ . Increasing the number of iterations by one allows to improve the power efficiency (approx. 0.5 dB at SER =  $10^{-4}$ ) such that the iterative VA outperforms the VA with two delay elements. The exact results for the iterative VA depend on the shape of the overall impulse response which changes with the roll-off factor. For practical values  $\beta > 0.2$ , we found the differences to be only marginal.

## VI. PASPR AND SPECTRUM USAGE

In the previous sections, we introduced several methods to reduce the PASPR of a signal and discussed their power efficiency. Some methods may have a negative impact on the bandwidth, but a wider spectrum may be tolerable, if the gain

TABLE II  
COMPLEXITY COMPARISON OF  
SI DEMODULATION ( $M = 64$ )

Algorithm	$\Xi$
Viterbi, $\nu = 1$	4096
Viterbi, $\nu = 2$	262144
Viterbi, RSSE	16384
It. Viterbi, $\nu_{\max} = 2$	4221
It. Viterbi, $\nu_{\max} = 3$	4846

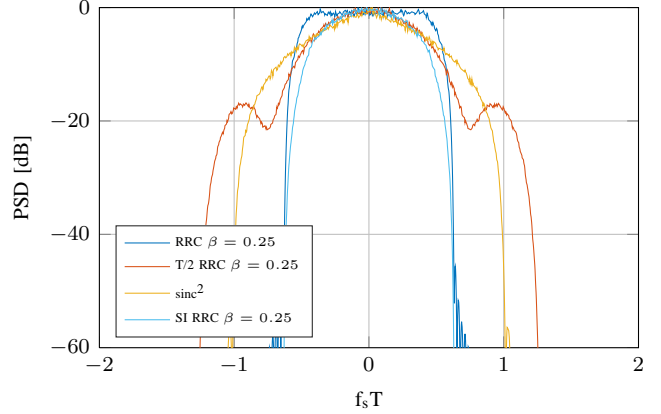


Fig. 8. Occupied spectra of different pulse shaping methods. The spectra are calculated for a  $n = 4$  antenna system.

in PASPR is substantial. In this section we discuss how much PASPR reduction can be achieved and how the corresponding spectrum behaves.

Our baseline is a root raised cosine (RRC) pulse shaping filter with roll-off factor  $\beta = 0.25$ . The comparison of bandwidth and PASPR is given in Figs. 8 and 9, respectively. In these plots, RRC and  $\text{sinc}^2$  describes conventional pulse shaping (see Sec. IV for  $\text{sinc}^2$  pulse shaping), T/2-RRC describes pulse shaping at twice the symbol rate and pulse shaping mixed with SI is named SI RRC (see Sec. V).

The general result regarding bandwidth and PASPR is the following:  $\text{sinc}^2$  pulse shaping is the simplest way to reduce the PASPR at the cost of increased bandwidth. T/2-RRC can reduce the PASPR even further, but it also requires even wider bandwidth and some receiver complexity. SI RRC on the other hand shows the least PASPR reduction, but it also reduces the occupied bandwidth slightly. For all RRC based methods, the well-known trade-off between bandwidth and roll-off still holds. Additionally, increasing  $\beta$  also improves the PASPR slightly.

In order to evaluate why  $\text{sinc}^2$  pulse shaping provides so much better PASPRs than a RRC even for one antenna, Appendix A provides some bounds and calculations on the PAPR of these pulse shapes. We show that the PAPR of  $\text{sinc}^2$  is equal to 1, whereas a sinc (which is closely related to RC and RRC) is generally unbounded.

## VII. BANDWIDTH EFFICIENCY OF PASPR REDUCTION

As a final comparison, we want to compare spectral efficiencies of the methods presented in this paper. Since some

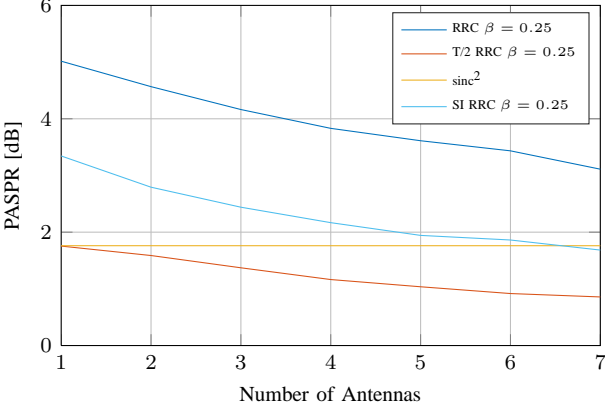


Fig. 9. Resulting PASPRs of different pulse shaping methods.

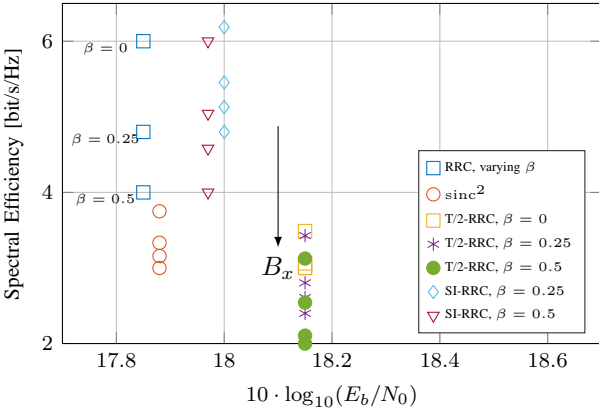


Fig. 10. Spectral efficiencies for different pulse shaping averaged over Rayleigh fading channels with  $n = 3$  antennas and a constellation size of  $M = 64$ . For all methods, except RRC, we plot the spectral efficiency based on the bandwidth  $B_x$  for a fraction  $x$  of the total energy. A target symbol error rate of  $\text{SER} = 10^{-4}$  was used.

pulse shaping methods have wide spectra, we also consider the bandwidth  $B_x$  which includes a fraction  $x$  of the total signal energy, e.g.,  $B_{99\%}$  is the bandwidth which holds 99% of the total energy of a signal.

In Fig. 10, the spectral efficiencies are plotted for a transmission system employing  $n = 3$  antennas and a constellation size of  $M = 64$  over a Rayleigh fading channel. As a baseline, a RRC with  $\beta = \{0, 0.25, 0.5\}$  is used. For all other pulse shaping methods, we plot the spectral efficiencies for  $B_x$  with  $x \in \{99\%, 99.9\%, 99.99\%, 100\%\}$  (the last one is of course the total bandwidth). The general result can be summarized as follows: All methods achieve the target symbol error rate of  $\text{SER} = 10^{-4}$  within a narrow band of approx. 0.3 dB. T/2-RRC shows both the worst power efficiency as well as the worst spectral efficiency, but it also achieves the largest gain in PASPR<sup>4</sup>.  $\text{sinc}^2$  has good power efficiency and a low PASPR, but also suffers from its large bandwidth. SI RRC shows a good trade-off between the other variants: The PASPR reduction is not as large, but there is almost no loss in spectral efficiency.

<sup>4</sup>Note that the gap for T/2-RRC to RRC vanishes as for a lower target SER, see Sec.V-A.

## VIII. CONCLUSION

We introduced PSKH and discussed different methods to generate data constellations on the hypersphere and their performance. Using PSKH constellations allows to use load-modulated transmitters which profit from the use of signals with low PASPR. For massive MIMO systems, a low continuous-time PASPR signal is easy to generate, but if only a handful of antennas is used, some PASPR reduction techniques have to be applied. For this reason, several low-PASPR pulse shaping methods were introduced and compared. They provide a trade-off between power efficiency, spectral efficiency and receiver complexity. It is possible to reduce the PASPR without sacrificing spectral efficiency, thus proving that load-modulation amplifiers are a valid approach not only for massive MIMO systems, but also if only a small number of antennas is employed.

## APPENDIX A

### PAPR OF SIGNALS USING $\text{sinc}$ AND $\text{sinc}^2$ PULSE SHAPING

*Theorem 1:* W.l.o.g. assume that an alphabet  $\mathcal{A} = \{a_0, \dots, a_{M-1}\}$ ,  $a_i \in \mathbb{R}$  with  $\max_i |a_i| = 1$  is given and an arbitrary data sequence with symbol rate  $1/T$  is used to generate a continuous signal

$$g(t) = \sum_{k=-\infty}^{\infty} a[k] * \text{sinc}\left(\frac{t - kT}{T}\right) \quad (15)$$

with  $a[k] \in \mathcal{A}$ . Then  $\max_t |g(t)|^2 = \infty$ .

*Proof:* W.l.o.g. we set  $T = 1$  and maximize  $|g(t)|$  instead of  $|g(t)|^2$ , which is achieved at the same point.  $\text{sinc}(t)$  has no sign changes in an interval  $(k, k+1)$  for  $k \in \mathbb{Z}$ , thus  $g(t)$  is maximized if all superimposed sinc functions have the same sign in a given interval and a coefficient with maximum amplitude. In the interval  $[0, 1]$ , this is achieved if we choose  $a[k] = -1$  if  $k$  is even and positive or odd and negative. Otherwise, we choose  $a[k] = 1$ . This gives

$$g(t) = \text{sinc}(t) + \sum_{k=1}^{\infty} (-1)^{k+1} \text{sinc}(t - k) + \sum_{k=-\infty}^{-1} (-1)^k \text{sinc}(t - k) \quad (16)$$

which is symmetric around  $\frac{1}{2}$ .

In order to find the maximum of  $g(t)$ , we can split the function into all pulses right of the symmetry axis and all those left of the axis. This gives us

$$g_1(t) = \sum_{k=-\infty}^{-1} (-1)^k \text{sinc}(t - k) + \text{sinc}(t) \quad (17)$$

$$g_2(t) = \sum_{k=1}^{\infty} (-1)^{k+1} \text{sinc}(t - k). \quad (18)$$

Note that due to symmetry, for  $0 \leq t \leq 1$  we have  $g_1(t) = g_2(1 - t)$  and  $g_1(1 - t) = g_2(t)$ . This allows to express the

derivative as

$$\begin{aligned} g'(t) &= (g_1(t) + g_2(t))' = (g_1(t) + g_1(1-t))' \\ &= g_1'(t) - g_1'(1-t) \end{aligned} \quad (19)$$

which is zero for  $g_1'(t) = g_1'(1-t)$ . This is obviously fulfilled for  $t = \frac{1}{2}$ . In fact,  $t = \frac{1}{2}$  is the only extremal value in the interval  $(0, 1)$ . This can be proven by looking at the monotonicity and concavity of each sinc pulse around its local maximum in this interval. We omit this part for the sake of brevity.

Because of  $2\text{sinc}(\frac{1}{2}) > 1$  we can conclude that there is no maximum at the boundary of our interval. We already chose  $|a[k]| = 1$ , thus the extremal value is

$$\max |g(t)| = \sum_{k=-\infty}^{\infty} \left| \text{sinc}\left(\frac{1}{2} - k\right) \right|. \quad (20)$$

In order to proof divergence of this value, we rewrite

$$\begin{aligned} \left| \text{sinc}\left(\frac{1}{2} - k\right) \right| &= \left| \frac{\sin(\pi(\frac{1}{2} - k))}{\pi(\frac{1}{2} - k)} \right| \\ &= \left| \frac{\cos(\pi k)}{\pi(\frac{1}{2} - k)} \right| = \frac{1}{|\pi(\frac{1}{2} - k)|}. \end{aligned} \quad (21)$$

We can thus rewrite the maximum as

$$\sum_{k=-\infty}^{\infty} \left| \text{sinc}\left(\frac{1}{2} - k\right) \right| = 2\text{sinc}\left(\frac{1}{2}\right) + \frac{2}{\pi} \sum_{k=2}^{\infty} \frac{1}{k - \frac{1}{2}} \quad (22)$$

which is essentially a harmonic series which is known to diverge.  $\blacksquare$

**Theorem 2:** Using the same assumptions as in Theorem 1, a continuous signal is generated as

$$g(t) = \sum_{k=-\infty}^{\infty} a[k] * \text{sinc}^2\left(\frac{t - kT}{T}\right). \quad (23)$$

Then  $\max_t |g(t)|^2 = 1$ .

*Proof:* W.l.o.g., we assume  $T = 1$  again. The proof's first steps are the same as above, but in this case we set  $a[k] = 1 \forall k$  because  $\text{sinc}^2$  is nonnegative for all input values. Because of  $2\text{sinc}^2(\frac{1}{2}) < 1$ , the maximum is either at  $t = 0$  or  $t = \frac{1}{2}$ . We know that  $g(0) = 1$ , so we take a closer look at  $t = \frac{1}{2}$ . Following the steps above gives us

$$\text{sinc}^2\left(\frac{1}{2} - k\right) = \frac{1}{\pi^2} \frac{1}{(\frac{1}{2} - k)^2} \quad (24)$$

which we can use to rewrite

$$\begin{aligned} g\left(\frac{1}{2}\right) &= \sum_{k=-\infty}^{\infty} \text{sinc}^2\left(\frac{1}{2} - k\right) \\ &= 2\text{sinc}^2\left(\frac{1}{2}\right) + \frac{2}{\pi^2} \sum_{k=2}^{\infty} \frac{1}{(\frac{1}{2} - k)^2}. \end{aligned} \quad (25)$$

Evaluating the sum-term using [25, p.9, eq. 0.234-2] gives

$$\sum_{k=2}^{\infty} \frac{1}{(\frac{1}{2} - k)^2} = 4 \cdot \left( \sum_{k=0}^{\infty} \frac{1}{(2k-1)^2} - 2 \right) = \frac{1}{2}(8 + \pi^2) - 8. \quad (26)$$

We can now use  $\text{sinc}^2\left(\frac{1}{2}\right) = \frac{4}{\pi^2}$  and insert it together with eq. (26) into eq. (25) to get

$$\sum_{k=-\infty}^{\infty} \text{sinc}^2\left(\frac{1}{2} - k\right) = 2 \cdot \frac{4}{\pi^2} + \frac{2}{\pi^2} \cdot \left( \frac{1}{2}(8 + \pi^2) - 8 \right) = 1 \quad (27)$$

## REFERENCES

- [1] F. H. Raab, P. Asbeck, S. Cripps, P. B. Kenington, Z. B. Popovic, N. Pothecary, J. F. Sevic, and N. O. Sokal, "RF and Microwave Power Amplifier and Transmitter Technologies - Part 1," *High Frequency Electronics*, vol. 2, no. 3, pp. 22–36, 2003.
- [2] M. A. Sedaghat, R. R. Müller, and G. Fischer, "A Novel Single-RF Transmitter for Massive MIMO," in *Proc. ITG Workshop on Smart Antennas*, 2015.
- [3] R. R. Müller, M. A. Sedaghat, and G. Fischer, "Load Modulated Massive MIMO," in *Proc. of IEEE Global Conference on Signal and Information Processing*, 2014.
- [4] M. A. Sedaghat, R. R. Müller, and C. Rachinger, "(Continuous) Phase Modulation on the Hypersphere," *IEEE Transactions on Wireless Communications*, vol. PP, no. 16, May 2016.
- [5] J. H. Conway and N. J. A. Sloane, *Sphere Packing, Lattices and Groups*. Springer, 1998.
- [6] N. J. A. Sloane, R. H. Hardin, W. D. Smith *et al.* Tables of Spherical Codes. [Online]. Available: <http://neilsloane.com/packings/>
- [7] P. Leopardi, "A partition of the unit sphere into regions of equal area and small diameter," *Electronic Transactions on Numerical Analysis*, vol. 25, pp. 309–327, 2006.
- [8] I. S. Dhillon and D. S. Modha, "Concept Decompositions for Large Sparse Text Data Using Clustering," *Machine Learning*, vol. 42, no. 1, pp. 143–175, January 2001.
- [9] J. M. Haile, *Molecular Dynamics Simulation: Elementary Methods*. Wiley, 1997.
- [10] G. Ungerboeck, "Channel coding with multilevel/phase signals," *IEEE Transactions on Information Theory*, vol. 28, no. 1, pp. 55–67, Jan 1982.
- [11] U. Wachsmann, R. F. H. Fischer, and J. B. Huber, "Multilevel Codes: Theoretical Concepts and Practical Design Rules," *IEEE Transactions on Information Theory*, vol. 45, no. 5, pp. 1361–1391, July 1999.
- [12] G. D. Forney and L.-F. Wei, "Multidimensional Constellations - Part I: Introduction, Figures of Merit, and Generalized Cross Constellations," *IEEE Journal on Selected Areas in Communications*, vol. 7, no. 6, pp. 877–892, August 1989.
- [13] J. Boutros and E. Viterbo, "Signal Space Diversity: A Power- and Bandwidth-Efficient Diversity Technique for the Rayleigh Fading Channel," *IEEE Transactions on Information Theory*, vol. 44, no. 4, pp. 1453–1467, July 1998.
- [14] F. Oggier, E. Bayer-Fluckiger, and E. Viterbo, "New algebraic constructions of rotated cubic lattice constellations for the rayleigh fading channel," in *Information Theory Workshop, 2003. Proceedings. 2003 IEEE*, March 2003, pp. 263–266.
- [15] E. Agrell and M. Karlsson, "Power-efficient modulation formats in coherent transmission systems," *Journal of Lightwave Technology*, vol. 27, no. 22, pp. 5115–5126, Nov 2009.
- [16] J. Leibrich and W. Rosenkranz, "Power efficient multidimensional constellations," in *Photonic Networks; 15. ITG Symposium; Proceedings of*, May 2014, pp. 1–6.
- [17] L. F. Wei, "Rotationally invariant trellis-coded modulations with multidimensional m-psk," *IEEE Journal on Selected Areas in Communications*, vol. 7, no. 9, pp. 1281–1295, Dec 1989.
- [18] G. D. Forney, "Maximum-likelihood sequence estimation of digital sequences in the presence of intersymbol interference," *IEEE Transactions on Information Theory*, vol. 18, no. 3, pp. 363–378, May 1972.
- [19] A. Viterbi, "Error Bounds for Convolutional Codes and an Asymptotically Optimum Decoding Algorithm," *IEEE Transactions on Information Theory*, vol. 13, no. 2, pp. 260–269, April 1967.
- [20] A. Duel-Hallen and C. Heegards, "Delayed Decision-Feedback Sequence Estimation," *IEEE Transactions on Communications*, vol. 37, no. 5, pp. 428–436, May 1989.
- [21] K. Shoemake, "Animating Rotation with Quaternion Curves," in *Proc. 12th Annual Conference on Computer Graphics and Interactive Techniques (SIGGRAPH)*, San Francisco, USA, July 1985, pp. 245–254.
- [22] I. E. Telatar, "Capacity of Multi-antenna Gaussian Channels," *European Transactions on Telecommunications*, vol. 10, no. 6, pp. 585–595, 1999.

- [23] W. H. Gerstacker, F. Obernosterer, R. Meyer, and J. B. Huber, "An Efficient Method for Prefilter Computation for Reduced-State Equalization," in *Proc.IEEE International Symposium on Personal, Indoor and Mobile Radio Communication (PIMRC)*,, London, September 2000, pp. 604–609.
- [24] M. V. Eyuboglu and S. U. H. Qureshi, "Reduced-State Sequence Estimation with Set Partitioning and Decision Feedback," *IEEE Transactions on Communications*, vol. 36, no. 1, pp. 13–20, January 1988.
- [25] I. Gradshteyn and I. Ryzhik, *Table of Integrals, Series, and Products*, 7th ed., A. Jeffrey and D. Zwillinger, Eds. Elsevier, 2007.